Separation Science and Technology
Publication details, including instructions for authors and subscription information:
http://www.informaworld.com/smpp/title~content=t713708471

Separation of a Five-Component Gas Mixture by Pressure Swing Adsorption

Peiling Cen[a]; Ralph T. Yang[a]
[a] DEPARTMENT OF CHEMICAL ENGINEERING, STATE UNIVERSITY OF NEW YORK AT BUFFALO, BUFFALO, NEW YORK

To cite this Article Cen, Peiling and Yang, Ralph T.(1985) 'Separation of a Five-Component Gas Mixture by Pressure Swing Adsorption', Separation Science and Technology, 20: 9, 725 — 747
To link to this Article: DOI: 10.1080/01496398508060701
URL: http://dx.doi.org/10.1080/01496398508060701

SEPARATION SCIENCE AND TECHNOLOGY, 20(9 & 10), pp. 725-747, 1985

Separation of a Five-Component Gas Mixture by Pressure Swing Adsorption

PEILING CEN and RALPH T. YANG*

DEPARTMENT OF CHEMICAL ENGINEERING
STATE UNIVERSITY OF NEW YORK AT BUFFALO
BUFFALO, NEW YORK 14260

Abstract

Bulk separation of a five-component mixture simulating coal gasification products was performed by pressure swing adsorption (PSA) using activated carbon. The PSA cycle consisted of four commercially used steps: (I) pressurization with H_2, (II) adsorption, (III) blowdown, and (IV) evacuation. Using this cycle, four products were obtained with a single PSA unit: H_2 (over 99.7% purity), CO, CH_4, and acid gas ($CO_2 + H_2S$). The first three products contained less than 0.001% H_2S, and the acid gas was suitable for sulfur recovery. A mathematical model incorporating equilibrium adsorption of mixture and mass transfer resistance (of CO_2) was found capable of simulating all steps of the PSA cycle. The model simulation results were in fair agreement with the experimental data. A fundamental understanding of the dynamics of the cyclic process was gained through the model.

INTRODUCTION

Pressure swing adsorption (PSA) is a gas separation process in which the adsorbent is regenerated by rapidly reducing the partial pressure of the adsorbed component, either by lowering the total pressure or by using a purge gas. In the original PSA cycle, invented by Skarstrom (*1*), two steps (adsorption and depressurization/purge) are carried out in two adsorbent beds operated in tandem, enabling the processing of a continuous feed. Since the Skarstrom cycle, many more sophisticated PSA processes have been developed and commercialized. It has recently attracted increasing interest because of its low energy requirements as well as low capital investment costs (*2*). State-of-the-art reviews of the

*To whom correspondence should be addressed.

 0149-6395/85/2009-0725$3.50/0

PSA processes have been made by Keller (*3*) and Cassidy and Holmes (*4*). In modern PSA processes, three or more beds are used to synchronize and accommodate steps additional to those in the Skarstrom cycle: cocurrent depressurization and pressure equalization. Vacuum desorption has been used in some PSA processes where an ultraclean bed is required. It also has been used for the purpose of desorbing a strong adsorbate (*5*). The two major commercial applications of PSA have been air drying and hydrogen purification. Most of the commerical processes are, however, for purification purposes rather than bulk separation, i.e., for mixtures containing high concentrations of adsorbates (more than 10% by weight according to Keller) (*3*).

Despite the increasing industrial use of PSA, theoretical understanding of the process is still in a primitive stage. Brief reviews of the theoretical developments have been recently made (*6*). Most of the published models are equilibrium models involving single adsorbate (*7–10*) or two or more adsorbates (*11–13*). The other models take into account the mass transfer resistance and require increased amounts of computation (*14, 15*). In bulk separation of multicomponent mixtures, pore-diffusion (*16*), equilibrium, and linear-driving-force models (*13*) have been developed in this laboratory which have been successfully used to simulate experimental data for binary and ternary mixtures.

As pointed out by Keller (*3*), there is an increasing need for developing PSA processes for bulk separation of multicomponent mixtures. The goal of this study was to establish the feasibility of using PSA for separating coal gasification products. One of the applications in coal gasification remains in the production of hydrogen, where the separation of hydrogen represents a major area for improvement. This paper presents PSA separation results of a simulated coal gasification product. It is shown that a single PSA unit is capable of both hydrogen separation and acid gas removal. The effects of adsorption pressure, feed rate, and end pressure of cocurrent desorption on the PSA separation have been determined. A mathematical model using the linear-driving-force approximation has been developed to simulate the PSA process. The model simulation results are in fair agreement with the experimental data.

EXPERIMENTAL

A single-column appartus (Fig. 1) was used which was capable of simulating all steps in a multicolumn PSA process. The gas mixture (premixed, supplied by Matheson) contained 1% (by volume) H_2S and

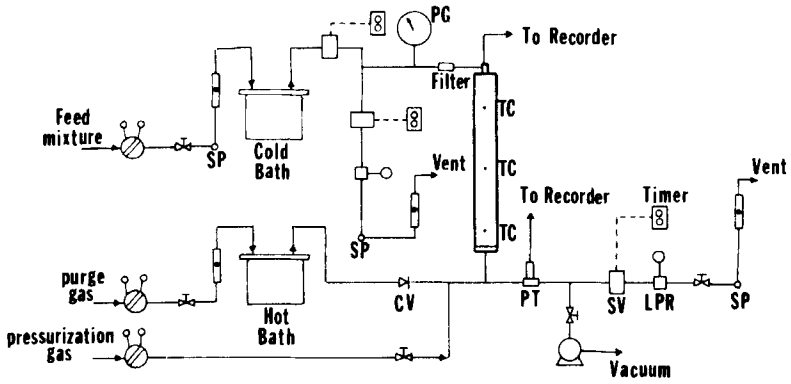

FIG. 1. Schematic diagram of apparatus for pressure swing adsorption. SP, sampling port; PG, pressure gauge; CV, check valve; PT, pressure transducer; SV, solenoid valve; TC, thermocouple; LPR, line pressure regulator. Not shown are the line connecting the upper end of adsorber to the pump, and the flowmeter downstream of the pump.

24.75% each of H_2, CH_4, CO, and CO_2. A commerical activated carbon (PCB carbon from Calgon in Pittsburgh) was used as the sorbent. The characteristics of the sorbent and the packed column are shown in Table 1.

The PSA cycle consisted of four steps:

Step I: H_2 pressurization (0.5 min)
Step II: High-pressure adsorption (6.5 min)
Step III: Cocurrent blowdown or desorption (9.5 min)
Step IV: Countercurrent evacuation (3.0 min)

The total time for each cycle was 19.5 min. The apparatus was highly automated. The only manual work involved product flow rate recording

TABLE 1
Adsorption Bed Characteristics

Bed inside radius, 2.05 cm
Bed length, 60 cm
Particle size, 0.028 cm
Bulk density, 0.498 g/cm^3
Particle density, 0.85 g/cm^3
Interparticle void fraction, 0.43
Intraparticle void fraction, 0.61
Total void fraction, 0.78
Heat capacity of carbon, 0.25 cal/g/°C

and sample collection and analysis. Pressure and temperature (at three axial locations) were continually recorded. The evacuation step was performed by a mechanical pump (to approximately 0.1 torr). A cyclic steady-state was reached after approximately 4 to 5 cycles, starting from a clean bed. The bed was insulated and the ambient temperature was 20°C.

EQUILIBRIUM ADSORPTION FROM MIXTURE

Single gas isotherms and equilibrium adsorption of five-component mixtures for the gas-solid system studied here have been measured in this laboratory (*17–19*). The single gas isotherms were correlated by a hybrid Langmuir-Freundlich isotherm:

$$q_i^* = \frac{q_{mi} B_i P^{n_i}}{1 + B_i P^{n_i}} \tag{1}$$

where

$$q_{mi} = a_i + b_i/T$$

$$B_i = \exp\,(c_i + d_i/T) \tag{2}$$

The values of *a, b, c, d*, and *n* are listed in Table 2. Also included in the table are the experimental heats of adsorption.

Several theories are available for predicting multicomponent adsorption from single isotherms (*6*). However, iteration is required in their application. The noniterative correlation, loading ratio correlation (LRC) (*20*), was selected in our PSA model to reduce the amount of computation. Furthermore, neither the theories nor the LRC can fit the

TABLE 2
Parameters for Loading Ratio Correlation (Eq. 3) and Heats of Adsorption

i	*n*	*a*	*b*	*c*	*d*	1/η	*H* (kcal/mol)
H_2	0.97	87.68	42392	−12.336	1219.3	0.40	2.6
CO	1.02	65.11	17992	−9.442	1286.3	1.00	2.6
CH_4	1.00	−0.76	40539	−10.245	1756.0	0.95	5.0
CO_2	1.00	−52.86	80000	−10.435	1978.0	0.80	5.6
H_2S	1.00	29.04	62947	−9.057	1725.2	2.50	5.6

high-pressure data (*17*). Thus, an empirical "interaction parameter," η, was used in the LRC equations:

$$q_i = \frac{q_{mi}B_i(Py_i/\eta_i)^{n_i}}{1 + \Sigma B_i(Py_i/\eta_i)^{n_i}} \tag{3}$$

The empirical values of η are also listed in Table 2. With the empirical values in Table 2, Eq. (3) was able to predict values to within 20% for all four components except H_2, as compared with Ritter's high-pressure data (*17*). The deviation for H_2 was substantially higher. However, this is not important since the amount of H_2 adsorption was nearly negligible in the PSA process.

MATHEMATICAL MODELS FOR PSA

Assuming no radial variations in concentration and temperature in the column, mass balance for the bulk gas and each component yields:

$$\frac{\partial uC}{\partial z} + \varepsilon \frac{\partial C}{\partial t} + \frac{\rho}{V_m}\frac{\partial q}{\partial t} = 0 \tag{4}$$

$$\frac{\partial uC_i}{\partial z} + \varepsilon \frac{\partial C_i}{\partial t} + \frac{\rho}{V_m}\frac{\partial q_i}{\partial t} = 0 \tag{5}$$

where $C_i = P_i/RT$ by assuming ideal gas behavior. Only $N - 1$ equations are needed for a N-component mixture in Eq. (5).

If the resistance to mass transfer is negligible, we have:

Equilibrium Model:

$$\partial q_i/\partial t = \partial q_i^*/\partial t \tag{6}$$

The mass transfer resistance, if important, can be approximated by using the following linear-driving-force (LDF) rates:

LDF model:

$$\partial q_i/\partial t = ka_i(q_i^* - q_i) \tag{7}$$

It is further assumed that the mass transfer coefficients, ka_i, are independent of temperature, pressure, and composition.

For energy balance, it is assumed that local equilibrium is instantaneous between the fluid and particles. We have:

$$\frac{\partial uCC_pT}{\partial z} + \varepsilon \frac{\partial CC_pT}{\partial t} + \frac{\rho}{V_m} \frac{\partial [q(C_{pa}T - H)]}{\partial t} + \rho C_{ps} \frac{\partial T}{\partial t} + \frac{2h}{r}(T - T_0) = 0 \tag{8}$$

where the last term represents the heat exchange with the ambient, which was not found negligible for a small column. The value of h was calculated and included the insulation layer. Four steps in series were accounted for: bed-to-wall, wall, insulation, and insulation-to-air. In addition, the simplifying assumption was made that the bed temperature was 40°C and that of the ambient 20°C. The heats of adsorption/desorption and heat capacities are:

$$H = \Sigma\, x_i H_i \tag{9}$$

$$C_p = \Sigma\, y_i C_{pi} \tag{10}$$

$$C_{pa} = \Sigma\, x_i C_{pi} \tag{11}$$

$$C_{pi} = A_i + B_i T + C_i T^2 + D_i T^3 \tag{12}$$

The parameters for Eq. (12) are listed in Table 3.

Equations (3)–(12) are solved numerically. The computation starts at the end of Step I of the first cycle, from a clean bed. The initial conditions, at $t = 0$, are:

$$y_{H_2} = x_{H_2} = 1.0$$

TABLE 3
Parameters for Heat Capacities

	A	$B \times 10^3$	$C \times 10^6$	$D \times 10^9$
H_2	6.483	2.215	−3.289	1.826
CO	7.373	−3.07	6.662	−3.037
CH_4	4.598	12.45	2.86	−2.703
CO_2	4.728	17.54	−23.38	4.097
H_2S	7.663	0.343	5.809	−2.81

$$y_i = x_i = 0, \qquad \text{for CO, } CH_4, CO_2, \text{ and } H_2S$$

$$P = P_f, \qquad T = T_0, \qquad q = q_0 \tag{13}$$

These conditions correspond to the column filled with H_2 at the feed pressure, P_f, and q_0 is the amount of H_2 adsorbed at P_f.

The boundary conditions for the subsequent cycles are:

Step II:
At $z = 0$ (the feed end)
$y_i = 0.2475$ for H_2, CO, CH_4, CO_2
$y_{H_2S} = 0.01$
$P = P_f, \quad T = T_0, \quad u = u_f$
At $z = L, \quad P = P_f$

Step III:
At $z = 0, \quad u = 0$
$t = t, \quad P = P(t)$

Step IV:
At $z = L, \quad u = 0$
$t = t, \quad P = P(t)$

Step I:
At $z = 0, \quad u = 0$
$t = t, \quad P = P(t)$

The final state in each cycle (Step II to Step I) is:

$$\text{At } t = \Delta t, \qquad P = P_f$$

The pressure history, $P(t)$, is recorded and expressed in quadratic forms. The pressure drop across the column is neglected. When $P(t)$ is used as an input, the product flow rate $u(t)$ is calculated. Conversely, $u(t)$ can be used as the input and $P(t)$ can be calculated. The use of $P(t)$ is, however, much more convenient in the computation and, in addition, it can be more accurately recorded.

The model was solved using an implicit finite difference method which was stable and convergent. Equations (4), (5), and (8) were expressed in implicit finite difference equations, incorporating Eqs. (3) and (6) or (7). In the computation, 25 space steps and 585 time steps were used for each PSA cycle. Temperature and concentrations were iterated into two separate loops. First, a set of C_i and T was assumed for each space segment. q_i were calculated from Eqs. (3) and (6) or (7). The value of u was then evaluated from Eq. (4). With these values, a new set of C_i was calculated from Eq. (5), which was compared with the assumed set. The

iteration was continued until y_i were within 10^{-4} of the assumed values. Equation (7) was used to calculate a new T, which was iterated until it was within 10^{-3} of the assumed T. All computations were performed in a VAX 780 computer. The computer time was approximately 10 min for a complete PSA cycle for a five-component mixture. Cyclic steady state was reached in approximately four to five cycles (which agreed with experimental results).

RESULTS AND DISCUSSION

By using the previously mentioned four-step PSA cycle, a simulated coal gasification product containing 1% (by volume) H_2S and 24.75% each of H_2, CO, CH_4, and CO_2 was separated. It was obvious that the mixture separation into five high-purity products by a single PSA unit was not possible. The goals of the separation were therefore to achieve: (1) a high-purity H_2, and (2) an acid gas which was suitable for further treatment such as sulfur recovery. The commercial sulfur recovery processes are capable of handling feeds containing only a few percent of H_2S and a much higher concentration of CO_2. Another goal for the separation was to produce "clean" or "sulfur-free" products, i.e., H_2 and CO/CH_4 (fuel) products. The range of operating conditions as well as the PSA cycle in this study were designed to achieve these goals.

Presentation and Analysis of a Typical Run

Typically four to five PSA cycles were required to achieve a cyclic steady-state from start-up of the process. In the experiments, steady-state was reached when the histories of pressure, temperature, concentration, and flow rate remained the same in each cycle. The experimental data of the 9th cycle of Run 5 are shown in Tables 4 and 5, and in Figs. 2 and 3. Table 4 shows the instantaneous flow rate and composition of the effluent from the column during the steady-state cycle. During the cocurrent blowdown step, Step III, the composition of the effluent varied from a H_2-rich early stage and CO-rich middle stage to a CH_4-rich later stage. Therefore, three cuts were made in Step III (IIIa, IIIb, and IIIc) to recover the three products. The time order of the products in the effluent was in agreement with the adsorptivities of single components. The results showed that four products could be obtained from a single PSA unit: H_2, CO, CH_4, and acid gas ($CO_2 + H_2S$). The volume-averaged product compositions and the volumes of all products are listed in Table 5. Table

TABLE 4
Cyclic Steady-State PSA Separation of a Mixture Containing 1% H_2S and 24.75% Each of H_2, CO, CH_4, and CO_2, for Run 5. The Experimental Data Are Compared with LDF Model Results. Feed/cycle = 38.4 L STP. P(feed) = 21.4 atm

		Flow rate (L/min)		Mole fraction of effluent (%)									
				H_2		CO		CH_4		CO_2		H_2S	
Step	Time (min)	Exptl	Calc	Exptl	Calc	Exptl	Calc	Exptl	Calc	Exptl	Calc	Exptl	Calc
II	2.0	2.11	2.61	100.00[a]	99.69	0.00	0.00	0.00	0.05	0.00	0.26		
	4.0	2.11	2.56	100.00	99.62	0.00	0.00	0.00	0.08	0.00	0.30		
	5.0	2.11	2.56	100.00	99.59	0.00	0.00	0.00	0.09	0.00	0.32		
	6.0	2.11	2.56	100.00	99.56	0.00	0.00	0.00	0.10	0.00	0.34		
IIIa	7.25	5.20	3.22	100.00	99.17	0.00	0.13	0.00	0.16	0.00	0.53		
	7.75	5.20	3.19	99.98	96.85	0.02	2.25	0.00	0.23	0.00	0.67		
IIIb	8.5	1.47	1.35	30.85	62.50	68.91	35.04	0.24	0.97	0.00	1.49		
	9.5	2.98	2.40	2.21	10.51	91.94	82.38	3.14	3.95	2.71	3.16		
	10.5	3.00	3.08	2.41	5.95	89.36	78.60	3.89	10.83	4.33	4.62		
IIIc	11.5	3.20	4.19	2.01	1.70	45.30	52.80	41.54	36.93	11.14	8.57		
	12.5	3.23	3.04	1.69	0.57	25.45	31.75	56.62	54.93	16.24	12.75		
	13.5	3.21	1.82	1.60	0.36	16.65	26.88	60.47	57.69	21.29	15.07		
	14.5	2.62	2.21	1.73	0.17	8.64	22.65	61.97	58.06	27.66	19.12		
	15.5	1.41	2.87	2.05	0.09	4.94	17.14	60.08	54.14	32.92	28.64		
	16.25	0.67	3.14	2.00	0.08	4.15	15.32	59.38	51.69	36.48	32.92		
IV	17.0	3.44	2.44	0.56	0.04	1.94	8.22	14.72	29.95	78.18	58.49	5.21	3.29
	18.0	3.07	3.05	0.93	0.00	1.06	5.59	17.89	27.06	75.74	63.78	4.37	3.56
	19.0	2.54	2.95	1.46	0.00	0.63	2.50	17.22	22.43	76.60	71.24	4.08	3.84

[a] 100.00% denotes over 99.99%.

TABLE 5
The Effect of End Pressure of Step III on Separation. The Compositions Are Steady-State Volume-Averaged Values. Run 5: Feed/cycle = 38.4 L STP, end P of III = 1.1 atm. Run 6: Feed/cycle = 38.2 L STP, end P of III = 0.6 atm. Pressure Histories Are Shown in Fig. 9. Feed Pressure = 21.4 atm

		Run 5						Run 6					
			Composition (%)						Composition (%)				
Step		Output (L)	H_2	CO	CH_4	CO_2	H_2S	Output (L)	H_2	CO	CH_4	CO_2	H_2S
II	Exptl	13.72	100.00					13.72	100.00				
	Equil	16.10	99.72	0.01	0.21	0.06							
	LDF	16.86	99.64	0.001	0.07	0.29		16.82	99.71	0.00	0.01	0.28	
IIIa	Exptl	5.20	99.98	0.02	0.00			5.11	99.84	0.10	0.06		
	Equil	3.86	99.43	0.02	0.46	0.09							
	LDF	3.62	98.58	0.70	0.16	0.56		3.43	98.89	0.57	0.04	0.50	
IIIb	Exptl	7.45	7.91	86.30	2.96	2.82		9.03	11.18	85.27	0.78	2.77	
	Equil	4.97	29.23	61.70	8.47	0.60							
	LDF	6.57	15.72	73.18	7.41	3.69		8.81	13.48	69.32	11.98	5.22	
IIIc	Exptl	14.00	1.73	22.35	55.30	20.62		16.97	2.18	14.44	51.97	31.41	0.001
	Equil	12.26	0.69	48.10	49.04	2.17							
	LDF	12.75	0.75	32.69	49.79	16.77		14.97	0.10	21.54	47.77	30.59	0.001
IV	Exptl	9.08	0.99	1.32	16.52	76.65	4.52	5.39	1.30	2.23	10.58	79.59	6.30
	Equil	12.86	0.03	3.89	24.05	69.01	3.02						
	LDF	10.29	0.04	4.51	24.99	66.82	3.64	5.93	0.05	2.12	20.55	71.76	5.52
Recovery, %	Exptl		90.40	98.74	83.90	69.39	100.00		84.80	98.83	93.97	43.36	99.46
	Equil		82.90	94.70	66.72	96.72	100.00						
	LDF		88.30	94.83	72.52	73.75	100.00		87.50	98.47	75.85	45.60	99.94

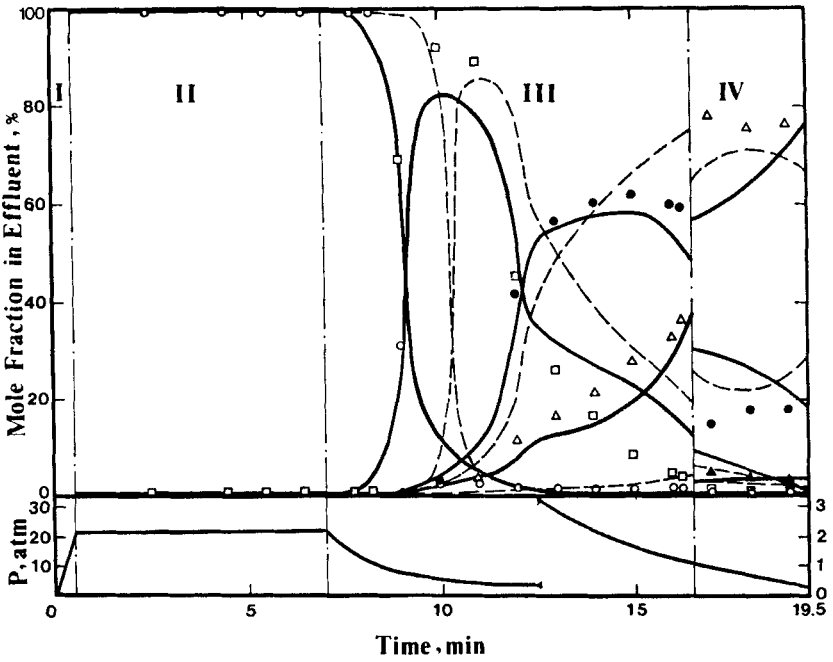

FIG. 2. Effluent concentrations in a steady-state PSA cycle for separating a 24.75/24.75/24.75/24.75/1.00 $H_2/CO/CH_4/CO_2/H_2S$ mixture with activated carbon (Run 5). The symbols are H_2 (○), CO (□), CH_4 (●), CO_2 (△), H_2S (▲) for the experimental data, Equilibrium model (dashed line), and LDF model (solid line).

5 also shows the product recovery for each component. The results showed that the goals of separation were achieved: An H_2 product at over 99.99% purity and 90.40% recovery, CO at 86.30% purity and 98.74% recovery, CH_4 at 55.30% purity and 83.90% recovery, and an acid gas containing 4.52% H_2S and 76.65% CO_2 were obtained. The H_2S content was not detectable with the gas chromatograph (which could detect 0.001% H_2S) in the H_2, CO, and CH_4 products. The throughput was 38.4 L STP/cycle, with 412 g carbon sorbent, and was in the range of commercial PSA operations.

The feed amount per cycle, at steady-state, was calculated by material balance:

$$\text{Feed/cycle} = \frac{\text{CH}_4 \text{ output in Steps II to IV}}{\text{Fraction of CH}_4 \text{ in feed}} \tag{14}$$

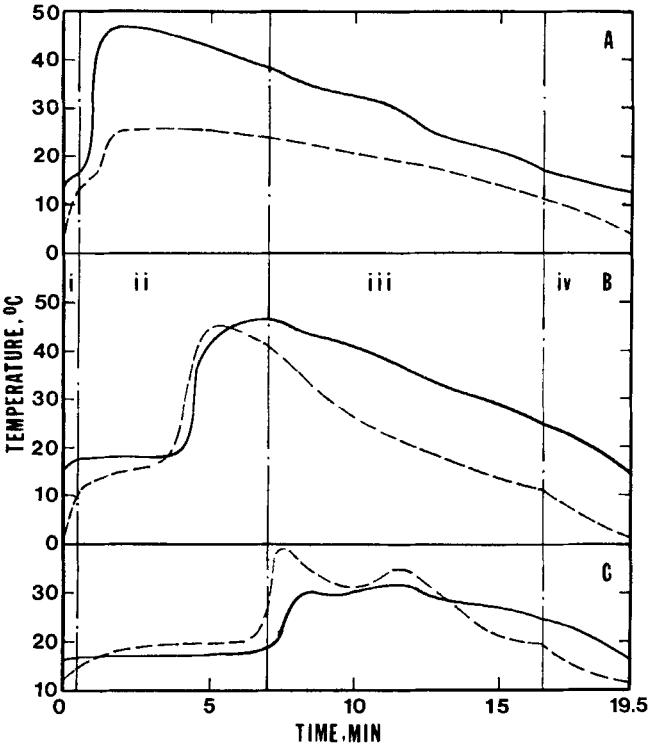

FIG. 3. Steady-state PSA temperature histograms (for Runs 5) at 12.7 cm (A), 33.0 cm (B), and 53.3 cm (C) from the top of the bed (60 cm height) which is the feed end. Solid line, LDF model; dashed line, experimental (Run 5).

Material balance at steady-state for all components was within a few percent. Since the amount of H_2 in feed equaled that of CH_4, the H_2 amount in Step I was calculated as:

$$H_2 \text{ in Step I} = H_2 \text{ output in Steps II to IV} - H_2 \text{ in feed} \tag{15}$$

The product recoveries were calculated as:

$$H_2 \text{ recovery} = \frac{H_2 \text{ output in II and IIIa} - H_2 \text{ input in I}}{H_2 \text{ in feed}} \tag{16}$$

$$CO(CH_4) \text{ recovery} = \frac{CO(CH_4) \text{ output in IIIb + IIIc}}{CO(CH_4) \text{ output in II to IV}} \tag{17}$$

$$\text{CO}_2(\text{H}_2\text{S}) \text{ recovery} = \frac{\text{CO}_2(\text{H}_2\text{S}) \text{ output in IV}}{\text{CO}_2(\text{H}_2\text{S}) \text{ output in II to IV}} \tag{18}$$

Figure 3 shows the temperature histories at three locations (at the center of the column) in the 9th cycle of Run 5. The temperature histories at points A (upper) and B (middle) simply reflect the movement of the wavefronts, with the peak indicating the crossing of the adsorbate wavefront. The wavefronts of the individual components were obviously not resolved. At the lower bed location (point C), two temperature peaks appear during cocurrent blowdown. The first peak indicates the readsorption of CO, which was desorbed from the upper bed, and the second peak refers to the readsorption of CH_4. The wavefronts of CO and CH_4 were clearly resolved during the blowdown step. These temperature peaks also corresponded well to the concentration profiles/histories in the column, as computed from model simulation.

The Equilibrium and linear-driving-force (LDF) models were both used. The results predicted (the Equilibrium model was a predictive model) by the Equilibrium model were in poor agreement with the experimental data, as shown in Fig. 2 and Table 5. The major discrepancy was in the CO_2 concentration. The experimental data consistently showed an earlier breakthrough of CO_2 in the PSA cycle than the Equilibrium model had predicted. This difference indicated that the mass transfer resistance for CO_2 in adsorption/desorption was significant. The CO_2 adsorption in Step II did not reach equilibrium. Thus, CO_2 concentration in the voids of the upper portion of the bed was high, and resulted in an early breakthrough during Step III. Therefore, the LDF model, i.e., Eq. (7), was used for CO_2, but Eq. (6) continued to be used for all other components in the LDF model. The mass transfer coefficient for CO_2 was empirically determined to be 0.2 s^{-1}. The results of the LDF model were in fair agreement with the experimental data, as seen in Fig. 2 and Tables 4 and 5. The temperature steady-state histories predicted by the LDF model, and compared with experimental data, are also shown in Fig. 3. The double peaks at the lower-bed point were also predicted by the model. As mentioned, the mass transfer coefficient for CO_2 was a fitting parameter. The empirical value of 0.2 s^{-1} was, however, not too far from the value of $15D/r_p^2 = 0.9$ s^{-1}.

Figures 4 to 7 show the LDF model simulation of the concentration profiles in the column at various times during a steady-state cycle in both gas and adsorbed phases. These profiles help understand the steady-state dynamics of the PSA process. Several observations are noted below. Concentration peaks for CO and CH_4 in both gas and adsorbed phases were formed in Step II, as shown in Figs. 4 and 5. The dynamics of Step

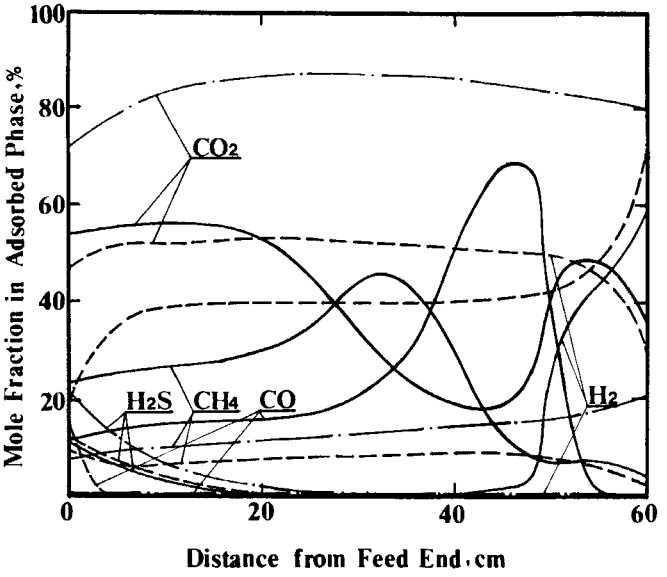

FIG. 4. The concentration profiles along the column in the adsorbed phase. End of Step IV (— ·), end of Step I (- -), end of Step II (——). Run 5.

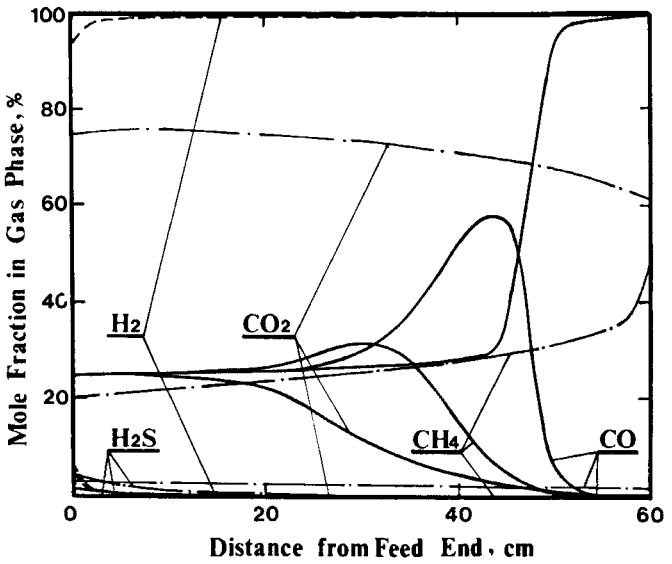

FIG. 5. The gas-phase concentration profile along the column predicted by the LDF model. End of Step IV (— ·), end of Step I (- -), end of Step II (——) Run 5.

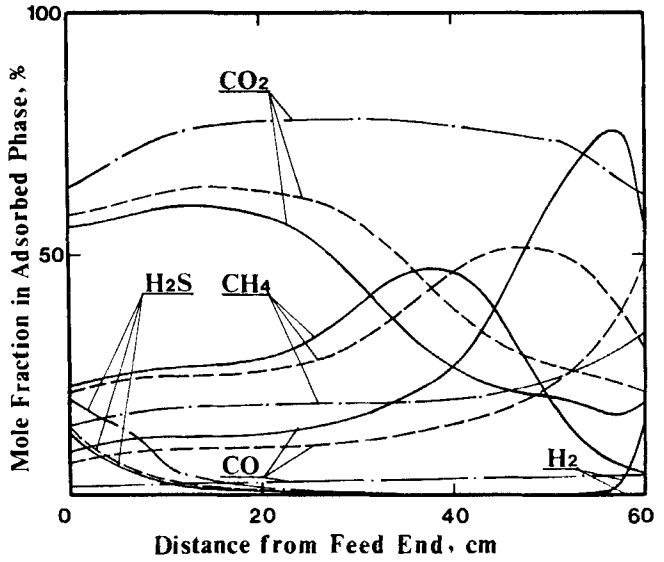

FIG. 6. The adsorbed-phase concentration profile along the column predicted by the LDF model during Step III. (——) 1.5 min, (- -) 4.5 min, and (— ·) 9.5 min from the start of Step III in Run 5.

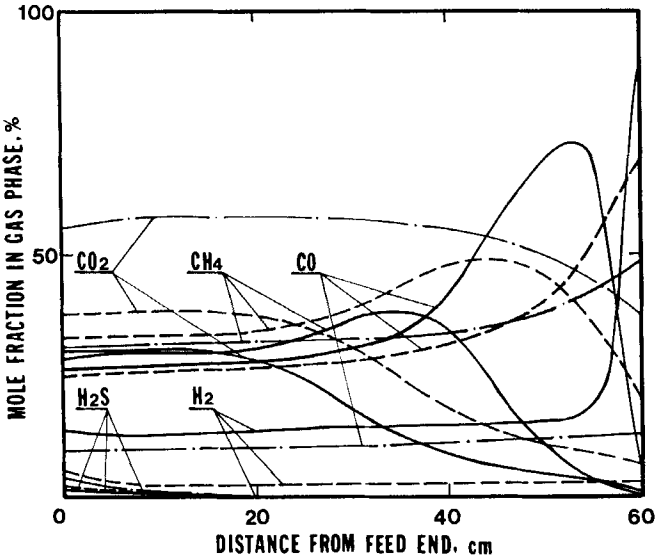

FIG. 7. The gas-phase concentration profiles along the column predicted by the LDF model during Step III, at (——) 1.5 min, (- -) 4.5 min, and (— ·) 9.5 min from the start of Step III in Run 5.

III are reflected in Figs. 6 and 7. The concentration peaks of CO and CH_4 moved toward the end of the column, and became more diffuse even though the distance between the peak locations increased. The diffuse and overlapped peaks resulted in poor separation of the two components. In Figs. 4–7, no clear concentration peaks were observed for CO_2. This finding was in agreement with the observation that no third temperature peak was seen at point C in Step III, Fig. 3. The CO_2 wavefront was much more diffuse than CO and CH_4, apparently due to the higher mass transfer resistance.

The relative adsorptivity (which indicates separability and is an opposite measure from the relative volatility used in distillation) is defined as

$$R_{ij} = q_i^*/q_j^* \tag{19}$$

where the q^* are from single gas isotherms. The R factors at 25°C and partial pressures in the feed mixture are $R_{CO/H_2} = 8.2$, $R_{CH_4/CO} = 1.7$, and $R_{CO_2/CH_4} = 2.0$. Based on the R values, the pair most difficult for separation was CH_4/CO, which agreed with the PSA results. The CH_4 product purity was further lowered by the lower mass transfer rate for CO_2. As a result, the CH_4 product purity only reached 60%.

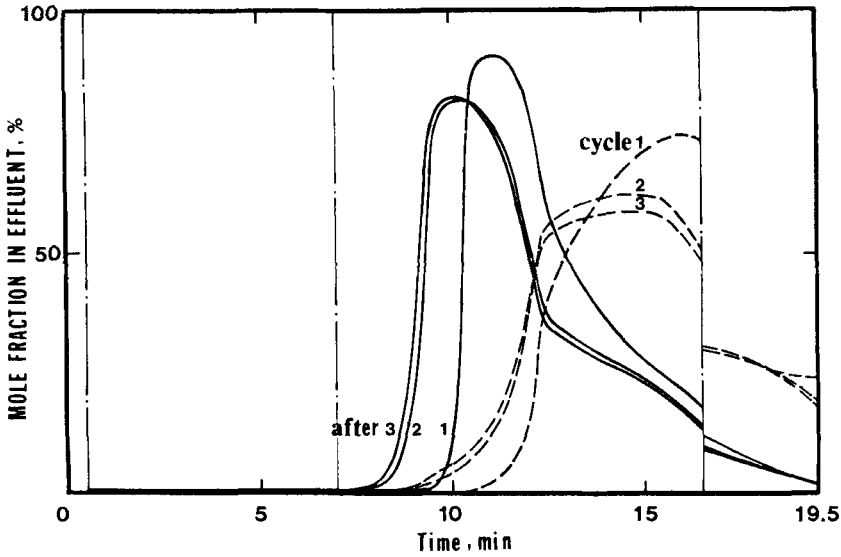

FIG. 8. The predicted transient CO and CH_4 concentration histograms by the LDF model. CO, solid line; CH_4, dashed line.

TABLE 6

Effect of End Pressure of Step III on Steady-State PSA at a Feed Pressure of 35 atm. Experimental vs Model Simulation by LDF Model. Run 2: Feed/cycle = 50.5 L STP, end P of III = 1.1 atm. Run 3: Feed/cycle = 50.7 L STP, end P of III = 0.8 atm.

		Run 2						Run 3					
			Composition (%)						Composition (%)				
Step		Output (L)	H_2	CO	CH_4	CO_2	H_2S	Output (L)	H_2	CO	CH_4	CO_2	H_2S
II	Exptl	18.27	100.00					18.27	100.00				
	Calc	24.73	99.75	0.00	0.02	0.23		24.75	99.73	0.00	0.01	0.26	
IIIa	Exptl	11.75	98.03	1.97				12.12	98.15	1.84	0.01		
	Calc	4.94	95.69	3.76	0.11	0.44		4.96	94.92	4.47	0.10	0.51	
IIIb	Exptl	12.94	5.34	75.27	15.45	3.94		12.94	4.79	71.64	18.39	5.17	
	Calc	12.82	14.23	63.70	17.53	4.54		12.87	13.95	63.45	17.57	5.03	
IIIc	Exptl	16.10	1.37	17.83	56.70	24.10		17.31	1.39	16.81	53.96	27.84	
	Calc	14.47	0.67	26.02	54.69	18.62		16.98	0.57	23.00	50.92	25.51	
IV	Exptl	10.21	0.69	1.37	13.42	80.12	4.41	8.30	0.96	1.08	9.88	82.65	5.42
	Calc	11.96	0.04	2.78	18.77	74.27	4.14	9.35	0.02	1.72	16.21	77.05	5.00
Recovery, %	Exptl		92.71	97.15	89.03	65.08	100.00		92.56	97.52	93.39	55.55	100.00
	Calc		85.38	95.83	81.83	72.58	100.00		85.65	96.93	87.75	58.70	100.00

The transient behavior, from start-up to steady-state, was well predicted by model simulation, as shown in Fig. 8. Due to the long cycle time, 19.5 min, a cyclic steady-state was reached after a small number of cycles. Figure 8 shows the rapid approach to steady-state.

Effects of Major Operating Variables in PSA

The effects of the operating conditions on the five-component PSA separation are indeed complex. Discussion on optimum operating conditions will not be meaningful until specific requirements are given for the separation. The effects of major operating conditions on the separation by the four-step PSA cycle were studied. The parameters studied were: adsorption (or feed) pressure, feed/cycle (or throughput), and the end pressure of Step III (blowdown). The experimental data and the LDF model simulation results are shown in Tables 5-7. The pressure histories of all runs are shown in Fig. 9.

Effects of End Pressure of Blowdown on Separation

The end pressure of Step III in the typical run, Run 5, was 1.1 atm. A lower end pressure would accomplish the following: (1) a higher CH_4 product recovery, and (2) a low pressure during the evacuation step, Step

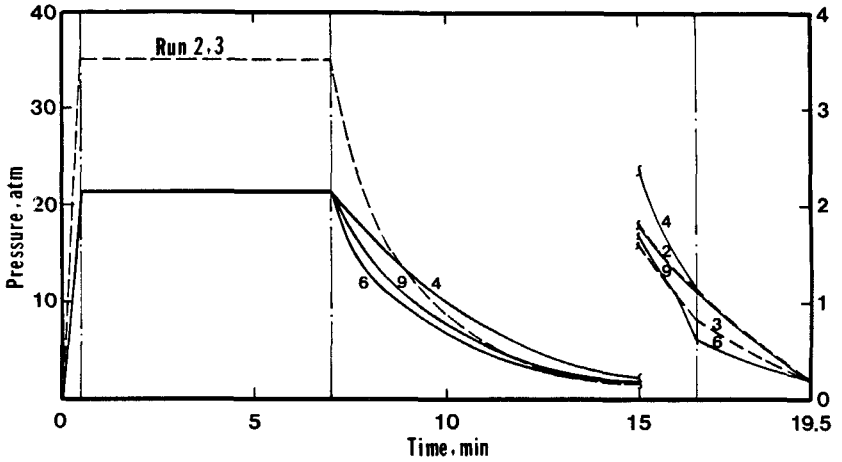

FIG. 9. The experimental pressure histories for feed pressure of 21.4 atm (solid line) and 35.0 atm (dashed line).

TABLE 7
Effect of Feed Rate on Steady-State PSA. Experimental Data Are Compared with LDF Model Simulation. Run 4: Feed/cycle = 48.4 L STP. Run 9: Feed/cycle = 31.8 L STP. The Pressure History Is Shown in Fig. 9

		Run 4						Run 9					
			Composition (%)						Composition (%)				
Step		Output (L)	H_2	CO	CH_4	CO_2	H_2S	Output (L)	H_2	CO	CH_4	CO_2	H_2S
II	Exptl	21.83	98.44	1.56				9.75	99.93		0.03	0.04	
	Calc	20.83	99.10	0.48	0.05	0.37		13.84	99.70	0.003	0.13	0.17	
IIIa	Exptl							7.76	99.72	0.00	0.18	0.10	
	Calc							5.72	99.00	0.28	0.36	0.36	
IIIb	Exptl	8.77	16.19	75.83	6.04	1.94		6.26	4.63	88.82	4.63	1.92	
	Calc	9.96	24.92	61.20	10.02	3.86		7.06	3.78	77.07	14.93	4.22	
IIIc	Explt	18.25	3.51	23.89	50.74	21.86		8.73	1.72	20.39	66.67	11.22	
	Calc	17.49	1.78	28.80	46.36	23.06		6.73	0.18	28.08	59.23	12.51	
IV	Exptl	10.87	1.34	1.40	20.47	72.46	4.33	8.57	1.17	1.40	20.42	73.40	3.62
	Calc	10.41	0.04	4.25	24.13	67.30	4.28	10.17	0.05	4.95	27.09	64.76	3.15
Recovery, %	Exptl		81.59	95.74	81.51	65.41	100.00		93.17	98.39	77.54	85.01	100.00
	Calc		77.04	95.35	78.31	60.92	100.00		97.00	93.39	64.37	84.76	100.00

IV, which in turn yields a higher product purity for H_2S. The end pressure of Step III was decreased by switching the effluent line to the mechanical pump line in the last ½ min of Step III. The end pressure of Step III in Run 6, with all other parameters nearly the same as in Run 5, was 0.8 atm. (The bottom plate of the column was a sintered steel plate which prevented a rapid lowering of pressure.) The results of Run 6, shown in Fig. 5, indicated that both H_2S product purity (increased from 4.52 to 6.30%) and CH_4 recovery (increased from 83.90 to 93.97%) were substantially increased. Table 6 shows a similar comparison of two runs at a higher adsorption (feed) pressure, 35 atm. The increase in H_2S product purity was significant because the costs for sulfur recovery in commercial processes are critically dependent on the H_2S feed concentration. The results showed clear benefits for a lower end pressure of Step III. The effects of the end pressure in Step III were clearly predicted by model simulation results as shown in Table 5 and 6.

Effects of Feed Rate

Since the time cycle was fixed, the feed rate was determined by the amount of feed per cycle. Runs 4, 5, and 9 were designed to determine the effects of feed rate as shown in Tables 5 and 7. The feed amount was in the following order: Run 4 > Run 5 > Run 9, keeping all other conditions nearly the same.

The effects of feed rate on separation were more exactly called the effects of bed utilization or coverage by adsorbates in the adsorption step, Step II. A cross examination of Tables 5 and 7 on Runs 4, 5, and 9 showed the separation of the first four components (H_2, CO, CH_4, and CO_2) was better at a lower feed rate. The H_2S product purity was, however, higher at a higher feed amount. The feed amounts were 31.8, 38.2, and 48.4 L STP/cycle, respectively, for Runs 4, 5, and 9.

Except for the least adsorbable component, H_2, there existed an optimal feed rate for each component; the optimal values were not the same for all components. They could, however, be predicted by model simulation. For the H_2S component, the optimal feed was apparently near 38.2 L STP/cycle, Run 5. For CO, the results of Run 9 (lowest feed) were much better than Run 4, but nearly the same as Run 5. For the H_2 product, results of Runs 5 and 9 were similar, but much better than Run 4, where the bed was nearly fully covered by the adsorbates during the adsorption step.

The fraction of the bed not covered by adsorbates in Step II was very important in producing high-purity products of the strongly adsorbed

components. A fundamental reason has been given (*13, 16*) by a total bed loading analysis. During Step III the clean bed performs the important function of readsorbing the desorbed components, and eluting H_2 out of the bed.

Effects of Feed Pressure

The effects of feed pressure should be more meaningfully discussed by the effects of bed utilization (in Step II). Nonetheless, results of two runs, Runs 2 and 4, may be compared from Tables 6 and 7. The total feed amounts per cycle were nearly equal, as with other conditions. The separation was better with a higher feed pressure, Run 2, except for the H_2S products which were similar. However, as noted, the bed was nearly fully covered by adsorbates in Step II in Run 4, whereas some clean bed was available in the column for readsorption in Step III in Run 2. The better separation in Run 2 was apparently attributable to the portion of clean bed. In general, the feed rate is dependent on the optimal bed coverage in Step II.

Effects of all operating variables discussed in the preceding were adequately predicted by the model simulation. However, the agreement between experimental data and model simulation was not entirely satisfactory. One of the reasons for disagreement involved the η values used for mixture adsorption. The value of η should be dependent on temperature, pressure, and composition as η_i approaches unity as $x_i = 1$. Constant η_i values were used in this work. Although axial dispersion was neglected in the model, the numerical solution inevitably included the effects of dispersion. Such effects have been discussed elsewhere (*13*). Another major possible cause for the deviation was the assumption that the pressure was uniform in the bed. A pressure gradient in the bed should result in a sharper wavefront during adsorption step and a more diffuse front during desorption. Inasmuch as the pressure gradient in fixed beds can be calculated, it should be included in a model for commercial design purposes.

SYMBOLS

A, B, C, D	constants in heat capacity equations
a, b, c, d	constants in adsorption isotherms
B_i	Langmuir constant, atm^{-1} or psi^{-1}
C	concentration in gas phase, mol/m^3

C_p	heat capacity of gas, cal/mol/K
C_{pa}	heat capacity of adsorbed phase, cal/mol/K
C_{ps}	heat capacity of adsorbent, cal/kg/K
D	effective pore diffusivity, cm^2/s
H	heat of adsorption, cal/mol
h	overall heat transfer coefficient, $cal/m^2/K/s$
ka	overall mass transfer coefficient, s^{-1}
q	adsorbed volume, m^3 STP/kg adsorbent
q_m	Langmuir constant, m^3 STP/kg adsorbent
N	number of components
n	loading-ratio-correlation constant
P	pressure, atm
R	gas constant
r	radius of column, m
r_p	radius of particle, m
T	temperature, K
t	time, s
u	superficial flow rate, m/s
V	volume, m^3
V_m	molar volume at STP
x	mole fraction in adsorbed phase
y	mole fraction in gas phase
z	height of column (= 0 at feed end), m

Greek Symbols

ε	fractional void in bed
ρ	bed density, kg/m^3 bed
η	modified LRC equation parameter

Superscript

*	equilibrium

Subscripts

f	feed
i	component i
0	initial

Acknowledgment

This work was supported by the U.S. Department of Energy under Grant DE-AC21-83MC20183.

REFERENCES

1. C. W. Skarstrom, *Ann. N. Y. Acad. Sci., 72*, 751 (1959).
2. H. A. Stewart and J. L. Heck, *Chem. Eng. Prog., 65*, 78 (1969).
3. G. E. Keller, *Industrial Gas Separations* (T. E. Whyte et al., eds.), American Chemical Society, Washington, D.C., 1983, p. 145.
4. R. T. Cassidy and E. S. Holmes, *AIChE Symp. Ser., 233*(80), 68 (1984).
5. S. Sircar, "Air Fractionation by PSA," U.S. Patent 4,329,158 (1982).
6. W. N. Chen and R. T. Yang, in *Recent Developments in Separation Science*, Vol. 9 (N. N. Li and J. M. Calo, eds.), CRC Press, Cleveland, 1985.
7. L. H. Shendalman and J. E. Mitchell, *Chem. Eng. Sci., 27*, 1449 (1972).
8. K. Weaver and C. E. Hamrin Jr., *Ibid., 29*, 1873 (1974).
9. G. F. Fernandez and C. N. Kenney, *Ibid., 38*, 827 (1983).
10. F. B. Hill, Y. W. Wong, and Y. N. I. Chan, *AIChE J., 28*, 1 (1982).
11. Y. N. Chan, F. B. Hill, and Y. H. Wong, *Chem. Eng. Sci., 36*, 243 (1981).
12. S. Nataraj and P. C. Wankat, in *Recent Advances in Adsorption and Ion Exchange* (Y. H. Ma et al., eds.), AIChE, New York, 1982.
13. P. L. Cen and R. T. Yang, *Ind. Eng. Chem., Fundam.*, In Press.
14. K. Chihara and M. Suzuki, *J. Chem. Eng. Jpn., 16*, 53, 293 (1983).
15. J. W. Carter and M. L. Wyszynski, *Chem. Eng. Sci., 38*, 1093 (1983).
16. R. T. Yang and S. J. Doong, *AIChE J.*, In Press.
17. J. A. Ritter, MS Thesis, State University of New York, Buffalo, 1984.
18. S. G. Byers, MS Thesis, State University of New York, Buffalo, 1983.
19. J. T. Saunders, MS Thesis, State University of New York, Buffalo, 1982.
20. C. M. Yon and P. H. Turnock, *AIChE Symp. Ser., 67*(117), 3 (1971).

Received by editor January 14, 1985
Revised April 15, 1985